Propagation Behaviors of Premixed Flames of R134a/CH_4/O_2/N_2 Mixtures

Byung Chul Choi[*,1], June Sung Park[2], Jae Ha Baek[1]

[1]Ship·Plant Technology Center, Korean Register of Shipping, Seoul, Republic of Korea
[2]Machinery Equipment Research Team, Korean Register of Shipping, Seoul, Republic of Korea

Abstract

The characteristics of the outward-propagating premixed flames of stoichiometric mixtures of R134a/CH_4/O_2/N_2 have been experimentally investigated in a constant volume combustion chamber. Three regimes of the expanding flames were categorized based on the flame behavior. In the typical regime, a conventional outward-propagating spherical flame was observed. When the concentration of R134a was relatively high, the buoyancy-induced regime, where the flame motion rises vertically and propagates outward, was observed. In addition, an intermediate transition regime existed between the two regimes.

Introduction

Substitution by a new refrigerant raises an important environmental and economical concern—the refrigerants already in use have to be collected and removed. In general, a waste refrigerant is disposed off by a direct combustion method using incinerators. The combustion of a high-GWP refrigerant generates CO_2, whose GWP = 1; thus, the amount of greenhouse gases is reduced, and the heat energy emitted during combustion can be recycled. In such an event, therefore, conventional incinerators need to be redesigned to accommodate the use of refrigerants as a fuel; hence, it is essential to understand the combustion characteristics of various refrigerants.

The premixed flames of mixtures in a mix of a base hydrocarbon such as methane and a refrigerant such as CFCs, HCFCs, and HFCs were frequently studied from the perspectives of their flammability limits, laminar burning velocities, and detailed reaction kinetics. Their fundamental characteristics were examined through the counterflow twin-flame technique [1-4], and in terms of flow geometry, their characteristics were examined using apparatus such as the Mckenna flat-flame burner [5], closed spherical vessel enclosed in a vacuum chamber [6], and Mache-Hebra nozzle burner as the Bunsen burner. Because such experiments focused on the chemical characteristics of the refrigerant-mixed mixtures, they were commonly performed with stabilized flames. Therefore, the flame dynamics related to the physical behaviors of the premixed flames that freely propagate in the refrigerant-mixed mixtures in the constant volume chamber need to be understood in a more comprehensive manner.

This experimental study purposes to examine the characteristics—laminar burning velocity, buoyancy-induced instability, and near-flammability limit—of spherical flames in a visualized constant volume chamber, where the spherical flames were variably mixed with R134a/methane/oxygen/nitrogen.

Experiment

The experimental apparatus consisted of a constant volume combustion chamber, which was equipped with an ignition unit, a schlieren system, a pressure sensor, and data acquisition equipment. Details of the experimental setup have been reported previously [7]. The combustion chamber was made of stainless steel of inner diameter 200 mm and length 220 mm; Fig. 1 shows a schematic diagram. Each end of the combustion chamber had a corrosion-resistant acrylic transparent observation window 150 mm in diameter and 40 mm in thickness. Two 0.5-mm-diameter tungsten electrodes with a 0.5-mm spark gap were installed at the center of the chamber, and they were connected to a capacitor discharge ignition system that supplies a high voltage of 8–10 kV.

A gas supplier was installed on the wall of the combustion chamber; it was equipped with an oil rotary vacuum pump. An absolute pressure sensor was connected to it in order to generate flammable gases under the initial premixture conditions by the partial pressure method. Commercially pure grade R134a (>99.90 %), methane (>99.95 %), oxygen (>99.99 %), and nitrogen (>99.99 %) were used to make gaseous premixtures and were left for 15 min until the ignition system began operating, to obtain homogeneous mixtures in the quiescent state.

The flames generated by a central ignition source were visualized using a Schlieren photography technique, for which a 300 W xenon light source, a pair of concave mirrors of 150 mm diameter were used. Images were captured using a high-speed camera operating at 10,000 frames per second with a resolution of 528 × 400 pixels. Simultaneously, variation in the pressure inside the chamber during combustion was measured by a quartz pressure sensor, which was equipped with a charge amplifier, and was recorded by a data logger.

In order to discharge the burned gases present inside the chamber, and to completely remove the residual gas

* Corresponding author: byungchul.choi@hotmail.com

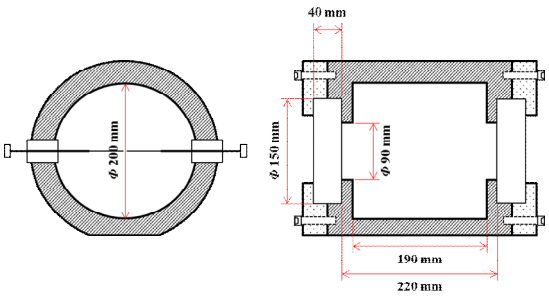

Fig. 1 Schematic of the cylindrical combustion chamber with central spark electrodes and observation windows on both vertical walls

and the condensate generated after combustion, the vacuum pump and fresh compressed air supplier were operated alternately several times. Thereafter, the unburned gases were reinjected for the next test. Note that the exhaust gas hydrogen fluoride (HF) was vented through a neutralization unit consisting of sodium hydroxide (NaOH) and water.

Result and discussion

In this study, the gaseous premixtures for the fuel and oxidizing agent were produced at atmospheric pressure and room temperature, where they remained in the equivalence ratio Φ = 1 following Dalton's law of partial pressures. Further, the chemical components of the R134a/methane/oxygen/nitrogen mixture were diversified for the experiment. The behaviors of the outward-propagating spherical flames generated by the combustion of the mixtures are reported in the following sections.

R134a(1,1,1,2-tetrafluoroethane), a fluorinated hydrocarbon, i.e., a hydrocarbon compound containing fluorine atoms, is expressed by the chemical formula $C_2H_2F_4$. The F/H ratio, i.e., the ratio of the number of F atoms to the number of H atoms, for $C_2H_2F_4$ is greater than 1. Because the gas is rich in F atoms, COF_2 or CF_4 as well as HF can be generated during combustion. [8,9]. Therefore, the global reaction of the flammable gas, which is a premixture of the fuel, R134a/methane, and an oxidizing agent, oxygen/nitrogen, at the stoichiometric air–fuel ratio is expressed as follows [9]:

$$R_R \cdot C_2H_2F_4 + (1 - R_R) \cdot CH_4 + (2 - 0.5 \cdot R_R) \cdot [O_2 + \{(1 - R_O)/R_O\} \cdot N_2] \rightarrow (1 + 0.5 \cdot R_R) \cdot CO_2 + 2 \cdot R_R \cdot HF + 0.5 \cdot R_R \cdot CF_4 + (2 - 0.5 \cdot R_R) \cdot \{(1 - R_O)/R_O\} \cdot N_2,$$

where $R_R = X_{R134a}/(X_{CH4} + X_{R134a})$, which is ratio of the molar fraction of R134a to the sum of the molar fractions of each component in the case of the binary fuel. Similarly, $R_O = X_{O2}/(X_{N2} + X_{O2})$, which is the molar fraction of the oxygen among the oxidizers.

Fig. 2 shows the temporal changes in the radius of the spherical flame and in the inner pressure, observed after ignition in a constant volume combustion chamber, for (R_O, R_R) = (0.20, 0.00). In the case of the initial premixture in the combustion chamber, a flame kernel formed between the electrodes, which were installed in the center, because of a high-voltage spark discharge

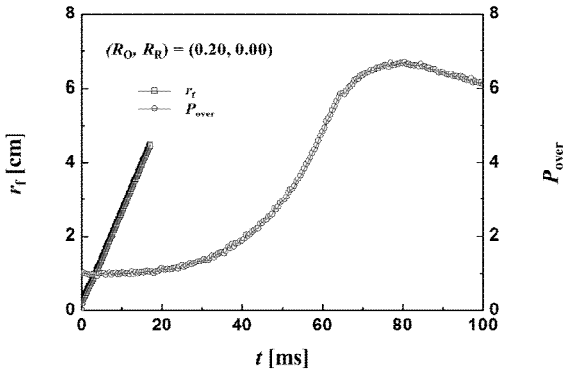

Fig. 2 Profiles of flame radius r_f and over-pressure P_{over} in terms of time t at (R_O, R_R) = (0.20, 0.00)

ignition (t = 0 ms). The spherical flames gradually propagated outward to the unburned gas. The radii of the spherically expanding flames r_f changed nonlinearly after ignition, and then increased linearly with time. The radius of the flames was visualized to be approximately r_f = 4.5 cm at t = 17 ms in the combustion chamber. As the premixed flames propagated up to the point where they could be observed, because the overpressure P_{over}, defined as P_a/P_0 where P_a is the actual pressure and P_0 the initial pressure, increased by a maximum of 2 %, the pressure change within the constant volume chamber could be disregarded [10]. Note that when the flames became large enough for observation, the overpressure rapidly increased during the entire combustion process, recording a peak value P_{over} = 6.84 at t = 80.5 ms.

Under the methane/oxygen/nitrogen mixture conditions at room temperature and atmospheric pressure within the cylindrical chamber, the behaviors of the flames, which were generated in the center after the ignition, propagating outward were practically the same as the typical behaviors of the flames of hydrocarbons [7]. The laminar burning velocities that were measured in accordance with the change in the equivalence ratio were confirmed suitable for the experiment and procedure adopted in this study, based on comparisons with the result of another study conducted by another group of researchers [7].

When the fixed oxidizing agent R_O = 0.20, the Schlieren images, which are shown in Fig. 3, were captured under fuel conditions R_R = 0.30 (a), 0.60 (b), and 0.75 (c) at specific elapsed times. Fig. 3a shows the typical behaviors of the spherical flames propagating to the inner wall from the center of the chamber as the time increased from 10 ms to 30 ms. The flames appeared to propagate as a perfect sphere; however, the images of the flames at 30 ms were observed to offset upward.

As shown in Fig. 3b, when the ratio of the refrigerant increased to R_R = 0.60, the flames, generated by the ignition, gradually rose in the reverse direction of the gravity while propagating outward between 20 ms and 70 ms. When the ratio of the refrigerant increased to R_R = 0.75, as shown in Fig. 3c, the propagation behavior

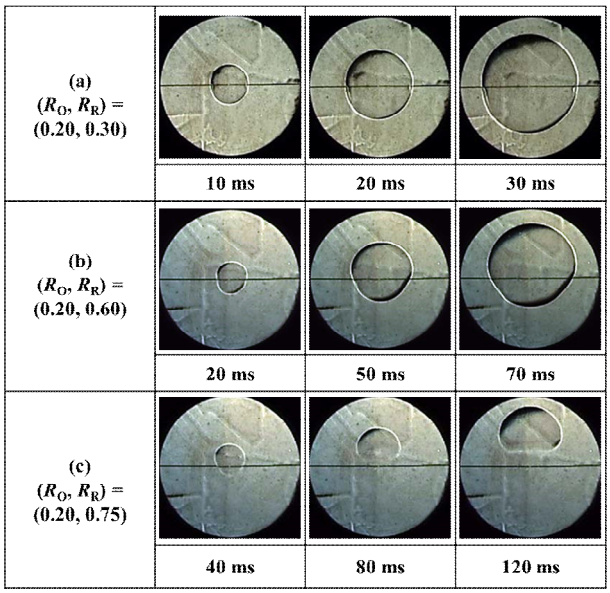

Fig. 3 Schlieren images for certain time intervals for R_R = 0.30, 0.60, and 0.75 at R_O = 0.20

of the flames showed that the upper part of the flames formed a hemisphere and rose far above the electrodes at the center between t = 40 and 120 ms. Moreover, the lower part of the flames is not very clear in the images, but it formed a conventional mushroom shape because the flame could not propagate downward against the flow induced by buoyancy. Similar behaviors have been observed in the case of lean methane–air mixtures as well because of buoyancy [11]. This will be further explained in the following sections.

Note that based on the Schlieren images shown in the Figs. 3a, b, and c, and under all experimental conditions in this study, it was confirmed the flames maintained a smooth surface without any wrinkles resulting from the turbulence on the surface of the propagating flames [12] or cellular structures resulting from the diffusional-thermal instability [13].

To analyze the characteristics of the flame behavior, the characteristic length of the spherical flame at a specific time was defined, all of which are shown in Fig. 4. The flame at a random moment t_1 was considered to have a dotted flame surface to the electrodes. After time Δt, the center of the rising flame at time t_2 was considered to rise vertically along the center of the

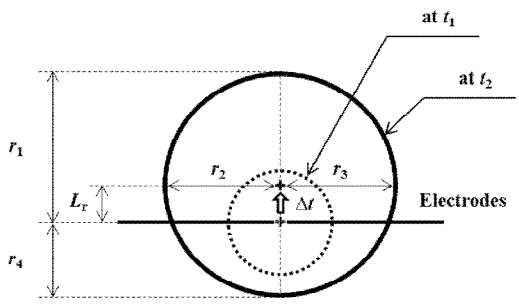

Fig. 4 Definitions of flame radii $r_{1\text{-}4}$ for the four directions and risen length L_r of the spherical flame

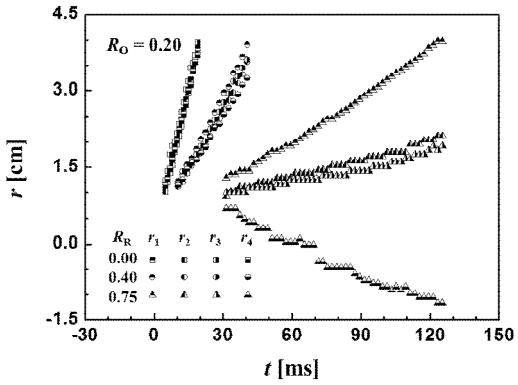

Fig. 5 Profiles of $r_{1\text{-}4}$ according to time t for R_R = 0.00, 0.40, and 0.75 at R_O = 0.20

combustion chamber, and the flame was considered to expand toward the solid-lined flame surface. The distances from the center, between the electrodes, to the flame surface in four directions was determined; the vertical radius to the upper surface was defined as r_1, and that to the lower surface, as r_4,; the horizontal radii to the left and right surfaces were defined as r_2 and r_3, respectively. As shown in Fig. 3c, as the flame rose, the vertical distance from the center of the spherical was defined as L_r. The length of the spherical flame characterized by time was automatically extracted through an image processing.

Fig. 5 shows the characteristics of the four radii, defined above, by time after the ignition (t = 0), where R_O = 0.20 under the sample conditions, i.e., R_R = 0.00, 0.40, and 0.75. To minimize the influence of the inner wall within the chamber in the later stage of combustion, the data for the time the flame growing up to 4 cm were considered good. Moreover, to nullify the effect on the ignition kernel in the early stage of combustion, the first 25 % of the minutes in each data set was excluded [14].

For pure methane where R_R = 0.00, the radii of $r_{1\text{-}4}$ overlapped linearly with time; in other words, the flame propagated uniformly in a pure sphere, and the interference caused by the cooling effect of the lateral electrodes was negligible. For the mixture added with a refrigerant at R_R = 0.40, the early flames were almost spherical, but the radii changed gradually with time. When r_1 = 4 cm, the difference between the radii were ±8.7 % at the maximum.

When the ratio of the refrigerant increased to 0.75, the behaviors of r_2 and r_3 were almost the same with time even if the flame was slightly inclined to the left. As the velocity of flame propagation and the velocity of the rising flame overlapped, r_1 increased faster than r_f.

Therefore, because buoyancy minimizes horizontally [15], the flame radius to measure the propagation velocity was defined as $r_f = (r_2 + r_3)/2$ in this study. The distance from the center of ignition to the central point of the rising flame could have been defined as $L_r = r_1 - r_f$. Although the early data set of r_4 was partially filtered as shown in Fig. 5, r_4 on the whole increased slightly after ignition and then decreased and became negative at

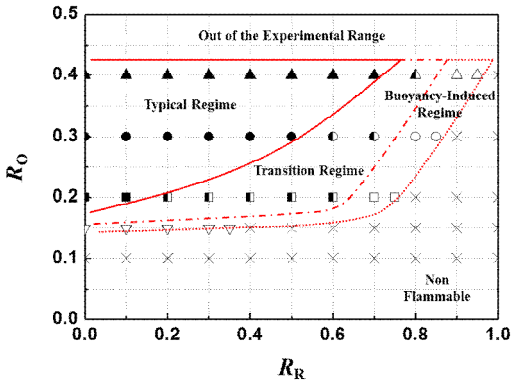

Fig. 6 Different regimes for the experimental conditions of R_R versus R_O

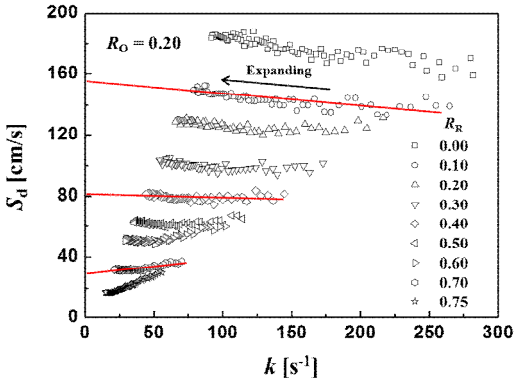

Fig. 7 The displacement speed S_d of the stretched flame front as a function of stretch rate k for the various R_R conditions at R_O = 0.20

t = 70 ms. This behavior was observed as, with time, the flame rose far above the electrodes installed in the center. Thus, $r_1 - r_4$ defined in this study, depicted well the behaviors of the flames shown in Fig. 3.

Fig. 6 represents the mapping data collected as R_O and R_R changed during this experiment. Based on the dynamic characteristics of the flames, which were observed in the experiment, the outward-propagating flames were classified into three regimes. When (R_O, R_R) = (0.20, 0.00) as shown in Fig. 5, the initial conditions under which the flame shows the shape of a perfect sphere with time form the typical regime, which is represented by closed symbols. When (R_O, R_R) = (0.20, 0.75), the initial conditions under which the flame rises above the electrodes in the center, causing r_4 to be negative form the buoyancy-induced regime, which is by open symbols. The initial conditions between these two regimes form the transition regime, which is represented by semi-closed symbols.

The non-flammable mixture conditions under which spark ignition is unable to generate a flame are represented by the symbol X. Note that the ranges of the R_R of the three regimes varied with the oxygen concentration of R_O. When R_O = 0.20, the typical regime occurs when R_R < 0.2, where this range is narrower than that of the entire flammable range. The ratio of the transition regime within the flammable limit when R_O = 0.40 decreased, while the range of the typical regime increased up to R_R < 0.80. On the other hand, under the initial conditions for the oxygen-enriched oxidizing agents of $R_O \geq 0.5$ and most of the R_R, an excessive rise in flame temperature could thermally deform the electrodes; hence, the initial conditions were eliminated in this study. In the following sections, the characteristics of the flame by each regime will be analyzed in detail for the initial conditions of R_O = 0.20, 0.30, and 0.40, in which the three regimes exist in accordance with R_R.

In the experiment, the flame front velocity of the outward-propagating spherical flames were obtained from the schlieren images using the pre-defined r_f as a temporal function, and the unstretched laminar burning velocity (or laminar flame speed), with which the flame propagates toward a quiescent unburned mixture, was deduced through the constant pressure method that was suggested by the previous studies [16-20], as described in below.

From the refined data on the radius of flame versus the time, as shown in Fig. 5, the variation in the displacement speed of the stretched flame front S_d in accordance with the stretch rate k for the spherical flame is replotted in Fig. 7. Following Bradley et al. [16-19], S_d can be deduced from the time rate of change of the radius of the instantaneous flame.

$$S_d = \frac{dr_f}{dt}$$

The flame radius r_f for the burned gas, extracted by the Schlieren technique during deduction of S_d, was considered the isotherm that is 5 K above the temperature of the reactants, and the error of the flame thickness was considered as the cold front and disregarded [16,17]. The time derivative k of the logarithm for the surface area of the flame A_f in the spherically expanding flame is generally defined as follows [16-20].

$$k = \frac{1}{A_f} \cdot \frac{dA_f}{dt} = \frac{2}{r_f} \cdot \frac{dr_f}{dt} = \frac{2}{r_f} \cdot S_d$$

When (R_O, R_R) = (0.20, 0.10), the flame, generated upon ignition, propagated spherically, and the stretch rate within the certain time limits decreased to 90 s^{-1} from 270 s^{-1}, while the displacement speed increased to 190 cm/s from 160 cm/s. As R_R gradually increased, the range and the magnitude of the stretch rate as well as the displacement speed decreased. Note that when R_R = 0.40, the gradients of the S_d values for k were very close to 0, and the gradients were negative for R_R > 0.40, which is a rather low range of the stretch rate; the gradients were positive for R_R < 0.40, a higher range of the stretch rate.

For example, when R_O = 0.20, and when R_R = 0.20, 0.40, and 0.70, the linear regression results for the experimental data for the stretched flame speeds and the stretch rates can be expressed by the solid lines shown

in Fig. 7. The linear relationship is defined as follows [21].

$$S_u - S_d = L_b \cdot k ,$$

which is based on linear extrapolation for the plot of S_d against k; here, L_b is the gradient, which is the Markstein length of the burned gas, and S_u is the unstretched flame speed when $k = 0$.

The Markstein lengths that were experimentally determined for R_O = 0.20, 0.30, and 0.40 are presented in Fig. 8 as a function of R_R. L_b did not change with R_O, though R_R was, in overall, inversely related with L_b. In other words, L_b decreased as R_R increased. In particular, for R_O = 0.20, 0.30, and 0.40, the values of L_b turned negative from positive when R_R = 0.40, 0.60, and 0.70, respectively.

In general, the Markstein length shows the responsiveness of the flame to the influence of the stretch rate on the surface of propagating flame, and depending on the property of the reactant mixture, it may be positive or negative [21]. During flame propagation with near constant pressure, if the flame surface is smooth, the flame is stable with positive L_b, while it is unstable with negative L_b, if the surface of the spherical flame is distorted or has a cell structure. The unstable flame surface is not only mainly caused by the diffusional–thermal instability resulting from preferential diffusion of premixtures with different equivalent ratios of multicomponents, including hydrogen [13,22,23], but also caused by the hydrodynamic instability, which is influenced by the local difference between upstream and downstream velocities for flame propagation resulting from thermal expansion [24-26]. Here, the influence of the buoyancy of the flame can be disregarded.

In view of the above consideration, L_b turns negative from positive in accordance with R_R, as shown in Fig. 8, and this appears to agree well with the instability characteristic of the spherically expanding flames, which was caused by the variation in R_R observed in this experiment, as shown in Fig. 3. If so, this result could mean that the stretch effect was the main cause behind the typical spherical flame rising with the increase in R_R.

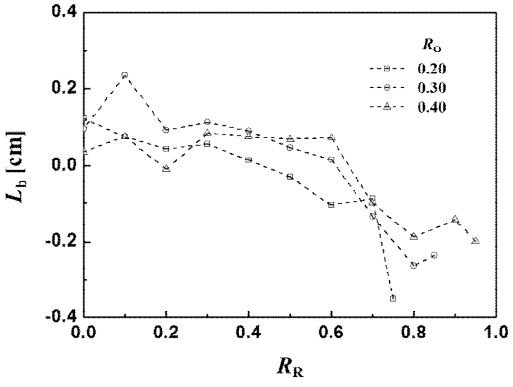

Fig. 8 Characteristics of the Markstein length L_b according to the variation in R_R at R_O = 0.20, 0.30, and 0.40

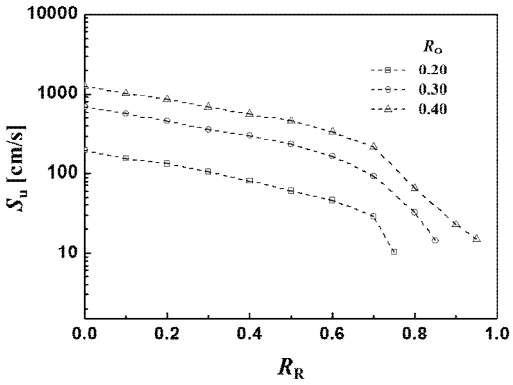

Fig. 9 The unstretched flame speed S_u according to the variation in R_R at R_O = 0.20, 0.30, and 0.40

However, no unstable structures were observed on the flame surface; further, the experimental characteristics of the Markstein length were insufficient to completely explain the three regimes and their boundaries as shown in Fig. 6. Therefore, this rising phenomenon will be discussed in detail in the future.

Fig. 9 shows the characteristics of the unstretched flame speed S_u extracted from the plot of stretch rate versus displacement speed of the flames against changes in R_O and R_R. As R_R increased to 1 from 0 for each R_O, S_u decreased monotonically, which agrees with the flame inhibition effect on the laminar burning velocity resulting from the mixture of the various chemical compounds [1-3,5,27,28], which consists of chlorine elements, as well as the fluorine in the methane–air mixture described earlier. Moreover, with the increase in R_O, S_u changed faster with R_R overall. This characteristic is similar to that of laminar burning velocity, which increases upon oxygen enrichment within the oxidizing agent in the stoichiometric premixed flame of methane [29].

As for the laminar burning velocity of the unburned mixture, the unstretched flame speed S_u changes first as per mass conservation for 1D planar steady propagation, as follows:

$$S_L = \frac{\rho_b}{\rho_u} \cdot S_u ,$$

where ρ is the gas density, and the subscripts b and u indicate burned and unburned mixtures, respectively. When the initial stoichiometric mixtures for R_O and R_R reached their equilibrium upon complete combustion, the specific volume υ for the density ratio was calculated using the EQUIL code [30] with the detailed kinetic mechanism developed by Burgess et al. [31]. The results are presented in Table 1. The ratios of the burned and unburned gases slightly decreased as R_R increased, but then increased again. This phenomenon was observed for each R_O. In spite of this, because the variation of the non-monotonic density ratio plays a minimal role in the conversion to S_L, S_L showed the same tendency as that of S_u—in other words, it decreased monotonically with R_R. This finding suggests

Table 1 The results of measurements of flame speeds and density calculations for the initial conditions.

R_O	R_R	v_b [cm^3/g]	v_u [cm^3/g]	ρ_b [g/cm^3]	ρ_u [g/cm^3]	ρ_u/ρ_b ($= v_b/v_u$)	S_b [cm/s]	S_L [cm/s]
0.20	0.00	6.51E+03	8.84E+02	1.54E-04	1.13E-03	1.36E-01	196.23	26.67
0.20	0.10	6.46E+03	8.60E+02	1.55E-04	1.16E-03	1.33E-01	154.14	20.53
0.20	0.20	6.42E+03	8.37E+02	1.56E-04	1.20E-03	1.30E-01	130.63	17.03
0.20	0.30	6.37E+03	8.13E+02	1.57E-04	1.23E-03	1.28E-01	104.73	13.36
0.20	0.40	6.33E+03	7.89E+02	1.58E-04	1.27E-03	1.25E-01	80.68	10.07
0.20	0.50	6.28E+03	7.66E+02	1.59E-04	1.30E-03	1.22E-01	60.34	7.36
0.20	0.60	6.24E+03	7.43E+02	1.60E-04	1.35E-03	1.19E-01	46.59	5.55
0.20	0.70	5.98E+03	7.21E+02	1.67E-04	1.39E-03	1.20E-01	29.23	3.52
0.20	0.75	5.77E+03	7.09E+02	1.73E-04	1.41E-03	1.23E-01	10.36	1.27
0.30	0.00	7.79E+03	8.89E+02	1.28E-04	1.12E-03	1.14E-01	686.71	78.45
0.30	0.10	7.69E+03	8.55E+02	1.30E-04	1.17E-03	1.11E-01	573.89	63.82
0.30	0.20	7.59E+03	8.22E+02	1.32E-04	1.22E-03	1.08E-01	457.95	49.55
0.30	0.30	7.50E+03	7.90E+02	1.33E-04	1.27E-03	1.05E-01	361.06	38.00
0.30	0.40	7.41E+03	7.58E+02	1.35E-04	1.32E-03	1.02E-01	305.30	31.23
0.30	0.50	7.33E+03	7.28E+02	1.36E-04	1.37E-03	9.94E-02	233.72	23.23
0.30	0.60	7.25E+03	6.99E+02	1.38E-04	1.43E-03	9.65E-02	165.53	15.97
0.30	0.70	6.93E+03	6.71E+02	1.44E-04	1.49E-03	9.68E-02	93.18	9.02
0.30	0.80	6.23E+03	6.44E+02	1.60E-04	1.55E-03	1.03E-01	32.56	3.36
0.30	0.85	6.01E+03	6.30E+02	1.66E-04	1.59E-03	1.05E-01	14.71	1.54
0.40	0.00	8.64E+03	8.94E+02	1.16E-04	1.12E-03	1.04E-01	1252.70	129.68
0.40	0.10	8.49E+03	8.50E+02	1.18E-04	1.18E-03	1.00E-01	1019.80	102.14
0.40	0.20	8.35E+03	8.09E+02	1.20E-04	1.24E-03	9.69E-02	852.08	82.56
0.40	0.30	8.21E+03	7.69E+02	1.22E-04	1.30E-03	9.37E-02	684.96	64.18
0.40	0.40	8.08E+03	7.32E+02	1.24E-04	1.37E-03	9.06E-02	565.68	51.25
0.40	0.50	7.96E+03	6.97E+02	1.26E-04	1.43E-03	8.75E-02	461.10	40.37
0.40	0.60	7.85E+03	6.64E+02	1.27E-04	1.51E-03	8.45E-02	338.56	28.62
0.40	0.70	7.52E+03	6.32E+02	1.33E-04	1.58E-03	8.40E-02	215.22	18.08
0.40	0.80	6.63E+03	6.02E+02	1.51E-04	1.66E-03	9.07E-02	65.12	5.908
0.40	0.90	6.10E+03	5.73E+02	1.64E-04	1.75E-03	9.39E-02	23.39	2.20
0.40	0.95	5.88E+03	5.59E+02	1.70E-04	1.79E-03	9.51E-02	15.14	1.44

that the difference between the classified flame regimes was caused by the decrease in the laminar burning velocity rather than by the variation in the density differences.

Conclusions

The characteristics of outward-propagating premixed flames ignited with a central spark ignition in R134a/methane/oxygen/nitrogen mixtures have been investigated experimentally in a visualized constant volume combustion chamber. Depending on the mixture ratios, the dynamic motions of the flames were classified into the typical regime and the buoyancy-induced regime, with an intermediate transition regime.

Acknowledgements

This research was supported by a grant from the LNG Plant R&D center funded by the Ministry of Land, Infrastructure and Transport (MOLIT) of the Korean government.

References

1. H. Wang, T.O. Hahn, C.J. Sung, C.K. Law, Combust. Flame 105 (1996) 291-307.
2. J.C. Leylegian, D.L. Zhu, C.K. Law, Combust. Flame 114 (1998) 285-293.
3. J.C. Leylegian, C.K. Law, H. Wang, Proc. Combust. Inst. 27 (1998) 529-536.
4. Y. Saso, D.L. Zhu, H. Wang, C.K. Law, N. Saito, Combust. Flame 114 (1998) 457-468.
5. D. L'esperance, B.A. Williams, J.W. Fleming, Combust. Flame 117 (1999) 709-731.
6. YU.N. Shebeko, V.V. Azatyan, I.A. Bolodian, V.YU. Navzenya, S.N. Kopylov, D.YU. Shebeko, E.D. Zamishevski, Combust. Flame 121 (2000) 542-547.
7. W.S. Song, S.W. Jung, J. Park, O.B. Kwon, Y.J. Kim, T.H. Kim, J.H. Yun, S.I. Keel, Int. J. Hydrogen Energy 38 (2013) 14102-14114.
8. W. Grosshandler, M. Donnelly, C. Womeldorf, Lean Flammability Limit as a Fundamental Refrigerant Property PhaseIII, NISTIR 6229 1998.
9. K. Takizawa, S. Kondo, A. Takahashi, A. Sekiya, K. Tokuhashi, ASHRAE Trans. 112 (2006) 459-468.
10. L.K. Tseng, M.A. Ismail, G.M. Faeth, Combust. Flame 95 (1993) 410-426.
11. P.D. Ronney, H.Y. Wachman, Combust. Flame 62 (1985) 107-119.
12. A. Hayakawa, Y. Miki, T. Kubo, Y. Nagano, T. Kitagawa, 8th KSME-JSME Thermal and Fluids Engineering Conference, 2012.
13. C.K. Law, O.C. Kwon, Int. J. Hydrogen Energy 29 (2004) 867-879.
14. A.P. Kelley, C.K. Law, Combust. Flame 156 (2009) 1844-1851.
15. U.J. Pfahl, M.C. Ross, J.E. Shepherd, K.O. Pasamehmetoglu, C. Unal, Combust. Flame 123 (2000) 140-158.
16. D. Bradley, P.H. Gaskell, X.J. Gu, Combust. Flame 104 (1996) 176-198.
17. D. Bradley, R.A. Hicks, M. Lawes, C.G.W. Sheppard, R. Woolley, Combust. Flame 115 (1998) 126-144.
18. X.J. Gu, M.Z. Haq, M. Lawes, R. Woolley, Combust. Flame 121 (2000) 41-58.
19. C.K. Law, C.J. Sung, Prog. Energy Combust. Sci. 26 (2000) 459-505.
20. F.A. Williams, Combustion Theory, 2nd ed., Addison Wesley, Redwood City, CA, 1985.
21. P. Clavina, Prog. Energy Combust. Sci. 11 (1985) 1-59.
22. J.K. Bechtold, M. Matalon, Combust. Flame 67 (1987) 77-90.
23. C. Prathap, A. Ray, M.R. Ravi, Combust. Flame 155 (2008) 145-160.
24. C.K. Law, Combustion Physics, Cambridge University Press, 2006.
25. S. Kwon, L.K. Tseng, G.M. Faeth, Combust. Flame 90 (1992) 230-246.
26. J.K. Bechtold, M. Matalon, Combust. Flame 127 (2001) 1906-1913.
27. G.T. Linteris, L. Truett, Combust. Flame 105 (1996) 15-27.
28. G.T. Linteris, D.R. Burgess, Jr., V. Babushok, M. Zachariah, W. Tsang, P. Westmoreland, Combust. Flame 113 (1998) 164-180.
29. C.E. Baukal, Jr., Oxygen-Enhanced Combustion, CRC Press LLC, Chapter 1, 1998.
30. R.J. Kee, G. Dixon-Lewis, J. Warnatz, M.E. Cottrin, J.A. Miller, SAND86-8246, Sandia National Laboratories, 1992.
31. D.R. Burgess, Jr., M.R. Zachariah, W. Tsang, P.R. Westmoreland, Prog. Energy Combust. Sci. 21 (1996) 453-529.